The Mechanical Environment of the Supraspinatus During Arm Elevation: A Three-Dimensional Finite Element Analysis

A THESIS SUBMITTED TO THE FACULTY OF THE UNIVERSITY OF MINNESOTA BY

Author: Anna Spracklin

Advisor: Dr. Paula Ludewig

IN PARTIAL FULFILLMENT OF THE REQUIREMENTS FOR THE DEGREE

OF MASTER OF SCIENCE

May 2019

Abstract

Rotator cuff pathology is extremely common, and can significantly reduce one's function in activities of daily living. The mechanisms of rotator cuff pathology are not well understood. This study aims to understand how supraspinatus stress and strain vary across a range of scapular plane elevation. Secondarily, to understand how imposing humeral head translations in the superior and inferior directions (±2 and ±5 mm) affect tendon mechanics. It was found that both stress and strain increased across the range of arm elevation. The posterior portion of the tendon underwent the greatest amount of strain, while the anterior portion near the footprint experienced the greatest levels of stress. With superior humeral head translation, the maximum stress and strain decreased, while inferior translation caused stress and strain increased. Further study is required to validate the finite element model. Alterations to the model may be done in order to address more clinical questions, such as how varying anatomy and subject specific kinematics affect rotator cuff mechanics.

Table of Contents

List of Tables

List of Figures

Introduction

Purpose of the Study:

The purpose of this study was to create and validate a finite element model of the glenohumeral joint (scapula, humerus, and supraspinatus) to examine the mechanical environment of the supraspinatus tendon over a range of arm elevation. Secondarily, to use the model to assess changes in mechanics due to humeral head translation in the superior and inferior directions across this range of motion.

Hypothesis/Research Question:

It is hypothesized that the stress within the supraspinatus tendon will be greatest toward end range arm elevation. In future work, the model will be validated against a cadaveric study, where surface strain will be compared to the strain predicted by the finite element model. Additionally, the tendon stress is expected to increase with inferior humeral head translation and decrease with superior translation. Intuitively, as the humeral head translates inferiorly, the tendon will be pulled down passively by the humeral kinematics while the muscle contraction will be pulling upward on the tendon to provide force for the rotational motion, causing additional tensile stress across the range of motion.

Significance:

It is thought that both anatomy and kinematics play an important role in development of rotator cuff pathology[1-3]. Kinematic factors may potentially be addressed by physical therapy, while certain anatomic variations may require surgical intervention to treat. Understanding how both kinematics and morphology affect the mechanics of the supraspinatus is important for prevention and treatment of rotator cuff tears, however, they are difficult to isolate in vivo, and the mechanics are difficult to quantify experimentally.

Many current experimental techniques, particularly to measure tissue mechanics, are invasive, making it particularly difficult to understand the healthy population where intervention is unnecessary [4-6]. Finite element analysis allows analysis of kinematics and morphology separately, and provides insight about the internal mechanics at play within the rotator cuff tendons.

Literature Review

The shoulder is a very unique joint in the human body. It is a perfect example of the intricate balance between stability and mobility. The glenohumeral joint is the most mobile joint in the human body, with the largest range of motion in three rotational directions. Because of the required mobility of the joint, the shoulder has limited passive stabilization, including a shallow glenoid fossa, labrum, and various glenohumeral ligaments [7]. Most of the stability of the joint comes from dynamic stabilization from the rotator cuff tendons. These muscles wrap around the humeral head and provide active stability by wrapping around the humeral head to pull and hold it in the glenoid [7].

Shoulder pain is the second most common musculoskeletal complaint [8]. One common cause of shoulder pain is presumed to be the development of rotator cuff tears. The supraspinatus is the most commonly injured [9]. Due to its line of action superior to the joint axis, the tendon is often under tension in order to stabilize the joint, even in a neutral position to counteract gravity [7]. The supraspinatus is subject to frequent tensile overload, leading to chronic overuse [7]. It has been proposed that the mechanisms of rotator cuff injury are due to a combination of intrinsic and extrinsic factors. Intrinsic mechanisms of rotator cuff injury are due to tissue degeneration, such as with aging, overuse, or changes in microvasculature [2]. Extrinsic mechanisms of rotator cuff injury involve mechanical

degeneration due to contact and compression of the rotator cuff tendons. For example, subacromial impingement, a proposed mechanism of supraspinatus tendon degeneration, occurs when the supraspinatus tendon comes into contact and is compressed by the coracoacromial arch [1]. In order to fully understand the mechanisms of rotator cuff injury, both intrinsic and extrinsic factors must be understood.

How glenohumeral kinematics and morphology influence extrinsic mechanisms of injury are not well understood. It is known that both have an impact on supraspinatus mechanics. Differences in scapular and humeral morphology have been theorized to be related to the development of rotator cuff tears. For example, the inclination of the glenoid, which is how far superiorly the glenoid faces, is thought to influence humeral head superior translation [10,11]. Similarly, one could intuit that a larger humeral head relative to the same subacromial joint space would decrease the subacromial space for the tendon to travel through, resulting in increased likelihood for subacromial impingement, and eventual development of a rotator cuff tear. There has been significant study in the area of acromial morphology, and different classifications of acromion (flat, curved, or hooked) have different likelihood of developing pathology [12]. Each person's anatomy is unique, so understanding how scapular and humeral morphology affect rotator cuff mechanics is important to understanding why some people develop rotator cuff pathology while others do not.

Glenohumeral kinematics are also known to have an effect on rotator cuff pathology. Ideally, motion at the glenohumeral joint would be pure rotation. Because the shoulder has such a large range of motion, stability must be compromised [2]. Humeral head translations are known to occur in subjects symptomatic of rotator cuff pathology as well

as healthy controls [13,14]. Superior/inferior translation in healthy controls has been seen to vary between two and five millimeters over the range of arm elevation, and between three and six millimeters in the anterior-posterior direction [13]. It is thought that humeral head translations impact rotator cuff pathology either by applying an additional traction on the tendon, increasing its tensile load, or by decreasing subacromial space, increasing the likelihood for contact and compression against the coracoacromial arch.

The relationship between anatomy and kinematics is not well understood. People may adapt their kinematics to alleviate symptoms. For example, if in a certain position, someone has significant subacromial compression, they may inferiorly translate their humeral head to reduce pain. The long-term effects of this translation on the soft tissue structures are not well understood. Finite element modeling can be utilized to parse out the effects of kinematics and anatomy independently to fully understand their effects individually, and ultimately be applied to a true in vivo condition, where the two are intertwined.

Finite element analysis is a computational method where space and time are discretized to convert complex partial differential equations into simplified linear systems of equations. In biomechanical applications, finite element analysis allows analysis of systems where in vivo measurements are invasive and difficult to control for all confounding variables. Finite element analysis is a non-invasive method to understand complex biomechanical systems, such as the glenohumeral joint.

Many finite element models have been created to model shoulder biomechanics – with some papers assessing the effect of anatomy or pathology on shoulder mechanics [15-23], while others analyze the effects of specific interventions or injuries [15,24-27]. There are

relatively few, however, that assess factors influencing rotator cuff injury. Inoue et al. investigated the mechanism and development of rotator cuff tears with respect to abduction angle [28]. Other investigators have created models to understand how the mechanics and loading capacity of the supraspinatus, infraspinatus, and teres minor are affected by various types of partial thickness tears [29-32].

One major limitation to finite element models is that numerous assumptions or constraints need to be made, and the only way to prove that the assumptions and limitations within the model are reasonable is to validate the model versus experimental data. Model validation varies from extensive, multi-subject cadaveric experimentation to validation relative to literature values. Grassi et al. performed an elaborate validation study of a femur model. The femurs were painted white and then speckled with an airbrush and digital image correlation was used to compute the principal strains and validate the strain output from the equivalent finite element model [33]. Typically, experimental methods to validate are done with either DIC and speckling, implanted beads, strain gauges, or markers to calculate the surface strain to compare with the strain predicted by the model [18,22,24,33-35].

Methods

Finite Element Model

An MR-image of a fresh-frozen cadaver shoulder was obtained using a Siemens 3T MRI Scanner (Siemens, Germany) (slice thickness = 0.7 mm, repetition time = 7.16 ms, echo time = 2.67 ms), and segmented using Mimics software (Materialise, Belgium) to create a three-dimensional model of the scapula, humerus, supraspinatus muscle, and supraspinatus tendon (*Figure 1*). The muscle-tendon junction was identified by changes in contrast in the MRI images to ensure accurate tendon size. The central tendon, where the

tendon continues deep into the muscle, was ignored for simplicity of the model. In order to maintain consistency across future subjects, these models were transformed from a global, mimics-based coordinate system to a scapular coordinate system defined by the z-axis pointing laterally from the root of the spine of the scapula to the center of the glenoid. The scapular plane was defined by this vector along with a vector pointing from the root of the spine of the scapula to the inferior angle. The x-axis was defined as the cross product of these two vectors, and the y-axis was defined by the cross product of the z- and x-axes. Because this model is a left shoulder, the z-axis points laterally, the x-axis points posteriorly, and the y-axis points superiorly. These changes in axes relative to the normal right-side coordinate system were accounted for when prescribing joint rotations.

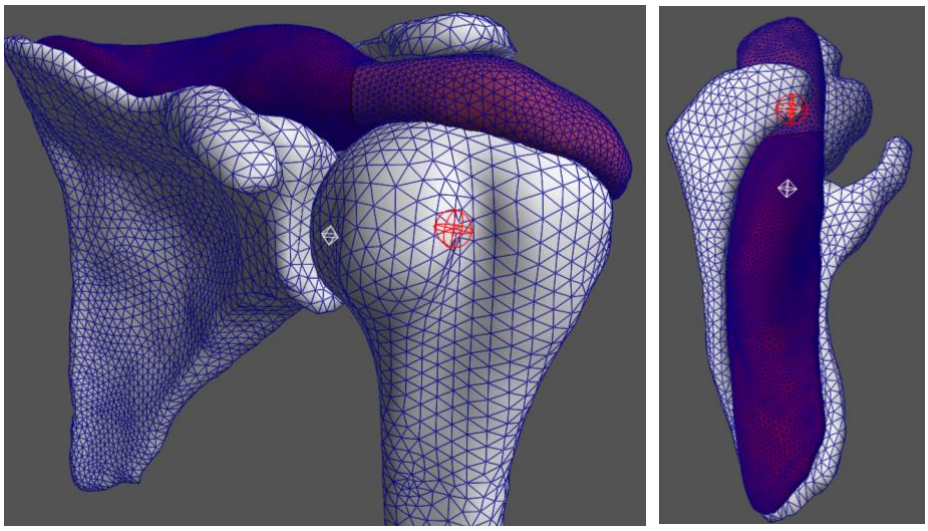

Figure 1. Model Geometry

Using subject-specific geometry, a finite element model was created for this subject using FEBio software (University of Utah). The scapula and humerus were modeled as rigid bodies, and meshed using Hypermesh software (Hyper-works 14.0, Altair, USA) with a linear tetrahedral mesh with an element size of three millimeters, in order to preserve geometry, while keeping the model reasonably simple. The supraspinatus muscle and

tendon were meshed with linear tetrahedral elements. The supraspinatus muscle and tendon had element sizes of one millimeter, based on a previously performed mesh convergence study, as this was the region of interest of the model.

The muscle was modeled as a solid mixture, with a transversely isotropic Mooney-Rivlin matrix, with muscle fibers pointed along its long axis (*Table 1*) [36]. The strain energy density equation for a Mooney-Rivlin matrix can be seen in *Equation 1*, below.

$$W = c_1(I_1 - 3) + c_2(I_2 - 3) + \frac{1}{2}K(\ln(J))^2 \quad (1)$$

Where c_is are constants, and I_1 and I_2 are invariants of the deviatoric part of the right Cauchy-Green tensor, defined as the transpose of the deformation gradient tensor multiplied by itself, and J is the determinant of the deformation gradient tensor. For this model, the muscle did not apply any force naturally. Instead, a force of 10 N was applied to the end of the muscle to simulate a force similar to that to be used in the experimental setup for validation.

The tendon was modeled as an uncoupled solid mixture, with a Mooney-Rivlin solid matrix (*Equation 1*), and power exponential fibers (strain energy density described in *Equation 2*) to mimic the material properties found by Lake et al. [6] (*Table 1*).

$$W = \frac{\zeta}{\alpha\beta}\left(\exp\left[\alpha(I_n - 1)^\beta\right] - 1\right) \quad (2)$$

Where I_n is the square of the fiber stretch in the fiber direction. The material properties were validated previously by mimicking a biaxial test, where a simulated square of the material is pulled along its edges, and the two-dimensional strain compared to experimental measures previously reported in the paper. A sliding, non-penetration contact was created between the scapula and the supraspinatus. This contact definition

allows the supraspinatus to slide over the supraspinatus fossa of the scapula, as it would occur in vivo, while inhibiting its ability to go through the bone to avoid deformation.

Table 1. Model Material Properties

Tendon Properties					
Mooney-Rivlin Matrix					
c1 [MPa]		c2 [MPa]		k [MPa]	
0.06		0.01		10	
Power-Exponential Fibers (uncoupled)					
alpha	beta	ksi [MPa]	k [MPa]	theta [deg]	phi [deg]
0	4.1	98.7	115	35.3	85.2

Muscle Properties						
Transversely Isotropic Mooney-Rivlin Matrix						
c1 [MPa]	c2 [MPa]	c3 [MPa]	c4 [MPa]	c5 [MPa]	k [MPa]	lambda
0.03	0.01	0.05	6.6	24.7	10	2
Prescribed Uniaxial Contraction						
Muscle Contraction (T0)		theta [deg]		phi [deg]		
0		35.3		85.2		

An arm elevation in the scapular plane was imposed according to joint angles from a study by Ludewig et al. tracking bone pins across various motions [4]. What we consider arm elevation is referred to as humerothoracic arm elevation, or how much the humerus is moving relative to the thorax. Humerothoracic (HT) elevation is composed of the motion of the sternoclavicular (SC), acromioclavicular (AC), and glenohumeral (GH) joints [7]. The contribution of the GH joint to HT elevation is roughly 2:1, compared to the motion from the AC and SC joints [7]. In this model, glenohumeral rotations are prescribed as they correspond to desired humerothoracic scapular plane elevation levels (*Table 2*). In order to correctly and uniformly impose kinematics, the scapular and humeral coordinate systems must be centered with respect to one another and set to a neutral position based on epicondyle position and humeral retroversion [37].

Because of the length of the humerus, the scan was not performed all the way to

the humeral epicondyles to prevent warping of the scan. Because of this, the humeral coordinate system was defined as a bicipital groove based coordinate system, as that point was easy to digitize in the three-dimensional space of the model. Massimini et al. studied the retroversion of numerous humeri to find that the average humeral torsion from epicondyles to bicipital groove [37]. This relationship was used to rotate the humerus to a "retroverted" position, which was really true neutral, where a vector connecting the humeral epicondyles is parallel to the frontal plane.

Table 2. Kinematic angles imposed in the model. HT – humerothoracic, GH – glenohumeral.

HT Elevation	**GH Elevation**	**GH Plane**	**GH Rotation**
30˚	-13˚	15˚	-34˚
60˚	-33˚	22˚	-48˚
90˚	-56˚	22˚	-61˚
120˚	-78˚	14˚	-65˚
150˚	-103˚	10˚	-65˚

The generalized joint rotations across the arm elevation are prescribed by an X Z' Y'' Cardan angle sequence (*Table 2*). The corresponding rotation matrices were applied to the three-dimensional bone models to rotate them through the range of motion (*Figure 2*). These rotation matrices were then turned into quaternions in order to prescribe the three-dimensional rotation to the FEBio interface.

The model was run under 3 conditions, 1) once the humeral head was centered, imposing glenohumeral rotations only. 2) Translations of ±5 millimeters were linearly imposed in the superior/inferior direction, such that at end range rotation the humerus had either translated 5 millimeters in the superior or inferior directions. 3) Finally, translations of ±2 millimeters in the superior/inferior direction were imposed.

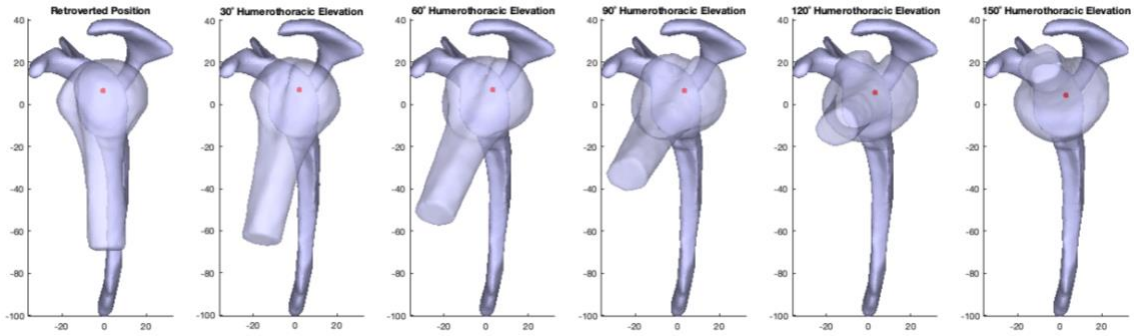

Figure 2. Glenohumeral Kinematic Positions. The red dot indicates the humeral head center.

Model Analysis and Post-Processing

The finite element method works by breaking up a large problem into many small, linear problems to estimate the global mechanics of the system. Prescribing a rotation of the humerus, the finite element solver, FEBio, will calculate nodal displacements. Using these displacements, the Lagrange Strain within each element is calculated.

Lagrange strain is defined as the deformation of the element relative to its undeformed configuration. In continuum mechanics, the Lagrange strain (E), is defined by *Equation 3*, below.

$$E = \frac{1}{2}(F^T F - I) \tag{3}$$

Where F is the deformation gradient tensor, defined as the matrix mapping the deformed geometry to the undeformed geometry, and I is the identity matrix.

This strain can be represented differentially (*Equation 4*),

$$E_{ii} = \frac{du_i}{dx_i};\ E_{ij} = \frac{du_i}{dx_j} + \frac{du_j}{dx_i} \tag{4}$$

where u_i is the displacement in the i-direction, and x_i indicates the unit vector in the i-direction [38]. Based on the displacements of the elements, these spatial calculations may be performed using the finite element shape functions.

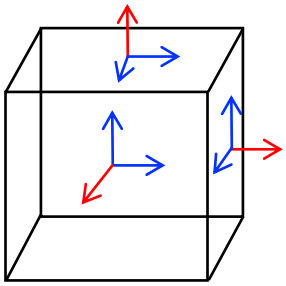

Figure 3. Differential Strain Element. Red arrows indicate normal strain directions, while blue represents shear directions.

On each element, strain may be represented as a combination of deformations normal to (normal) or in plane (shear) with the faces of the element (*Figure 4*). Often, von Mises strain, or effective strain, which is a scalar value describing the magnitude of strain on the element, is calculated to understand how likely these strains are to cause failure (*Equation 5*).

$$E_{vM} = \sqrt{E_{xx}^2 + E_{yy}^2 + E_{zz}^2 - E_{xy} * E_{xz} - E_{xy} * E_{yz} - E_{yz} * E_{xz} + 3(E_{xy}^2 + E_{xz}^2 + E_{yz}^2)} \quad (5)$$

Where E_{ii} indicates a normal strain, while E_{ij} indicates a shear strain.

Using the constitutive equations associated with the material definitions, the Cauchy stress may be calculated in order to better understand the true mechanics across the tendon. FEBio calculates the von Mises stress, also called effective stress (*Equation 6*), in order to provide a scalar value to describe the magnitude of stress in each element, and then applies a color map in order to visualize.

$$\sigma_{vM} = \sqrt{\sigma_{xx}^2 + \sigma_{yy}^2 + \sigma_{zz}^2 - \sigma_{xy} * \sigma_{xz} - \sigma_{xy} * \sigma_{yz} - \sigma_{yz} * \sigma_{xz} + 3(\sigma_{xy}^2 + \sigma_{xz}^2 + \sigma_{yz}^2)} \quad (6)$$

The effective stress and strain were calculated in each element throughout the range of motion. Looking at the peak stresses and strains in each angular position, as well as the color map for where these peaks are occurring, provides insight about how humerothoracic elevations and specific tendon locations that may impact supraspinatus tendon stress and strain.

Different areas of the tendon experience different mechanics. The footprint, which

is where the tendon attaches to the humerus, is responsible for the force transmission from the muscle to the humerus, so it experiences stress concentrations associated with this tension. The critical zone, which is one centimeter medial to the footprint, is a hypo-vascular zone that is commonly torn in supraspinatus tendon injury [39]. Analysis of these portions of the tendon separately may be helpful to understand how the mechanics at play differ between zones. Similarly, differences in material behavior has been described between the anterior and posterior portion of the tendon [6]. Although this wasn't modeled for simplicity sake, it indicates that the mechanics on the anterior and posterior portions of the tendon may be different. The effective stress and strain within each of these regions (anterior and posterior footprint, and anterior and posterior critical zone) was analyzed separately in order to understand how the mechanics differed between them.

Finally, in order to assess the effect of humeral head translations, the stress and strain were compared between various humeral head translation cases. The percent changes in stress and strain were calculated relative to the neutral case where the humeral head was held centered throughout the range of motion.

Validation Experiment

In order to validate the results of the model, the surface deformation of the tendon was intended to be compared between the model and a cadaveric study. The same fresh-frozen cadaver shoulder was dissected such that the scapula, humerus, rotator cuff tendons, joint capsule, and ligaments were all that remained. A custom jig was created such that the scapula could be mounted and weights attached to the rotator cuff tendons in order to center the humeral head (*Figure 4*). The scapula was positioned in a certain degree of upward rotation to mitigate the effects of gravity.

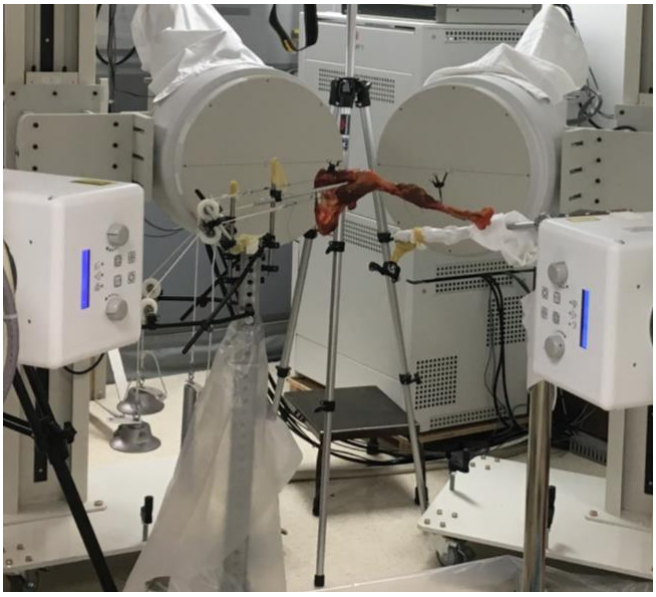

Figure 4. Experimental Setup

The humerus, attached to the scapula by the rotator cuff tendons, was placed as close as possible to the specific static positions throughout the range of scapular plane arm elevation imposed in the model (*Table 2*). In order to track true joint positions, 1.0 mm tantalum beads were inserted into the humerus and scapula, and glued in place using cyanoacrylate. The jig was used to hold the humerus in specific positions relative to the fixed scapula. The position was then captured using biplane fluoroscopy and the true joint position extracted.

To track the deformation of the supraspinatus tendon, speckles were painted onto the tendon using acrylic paint. Three DSLR cameras were set up such that the tendon was visible in at least two cameras throughout the range of motion. In order to calibrate the digital cameras, a three-dimensional calibration object was created and points were selected in each of the cameras to know where they were in space relative to one another.

Due to software limitations, the three-dimensional strain of the tendon was not able to be calculated. Two types of software – XMALab (Brown University), and MultiDIC

(Massachusetts Institute of Technology) – were used with no success to characterize the surface strain of the tendon in the various position. Both software packages seemed to struggle with calibration, where when a point was selected in one camera, it was projected to a very different point in the other cameras. MultiDIC was not able to correlate the window of speckles between cameras, making the digital image correlation impossible.

A future direction of this research will be to extract meaningful data from the experimental portion of this work in order to fully validate the model. Conceptually, using three cameras, as in this experiment, a calibration object may be used to understand the location of each camera with respect to one another. Either by using digital image correlation or defining points in all three cameras, points on the surface of the tendon should be identifiable by the cameras and the three-dimensional surface in each frame calculated and analyzed to obtain the surface strain across each position.

Results

Across the range of motion, FEBio calculates the von Mises strain within each element. It then applies a color map to visually describe field of strain over the surface (*Figure 5*).

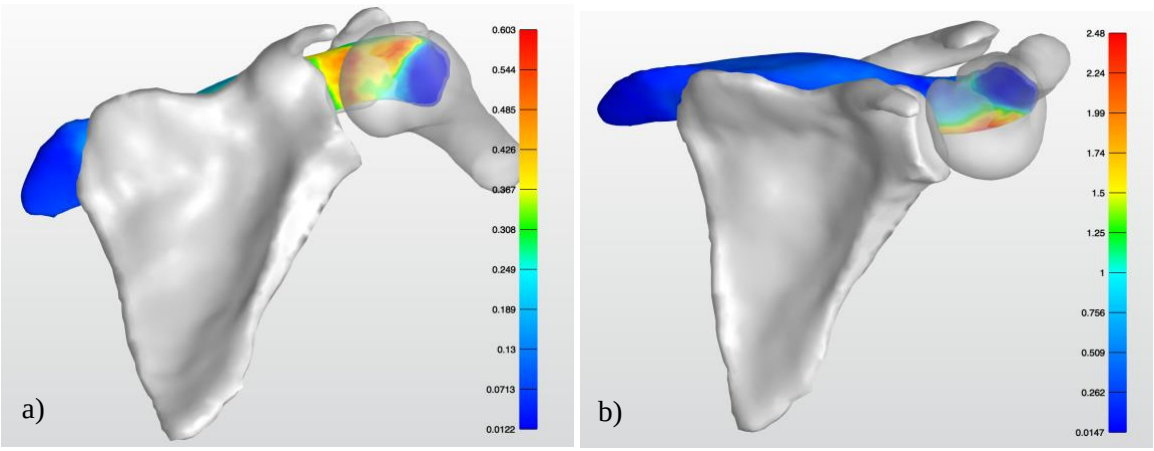

Figure 3. Effective Lagrange Strain on the tendon at a) 30 degrees and b) 150 degrees of Humerothoracic Elevation (Anterior View)

As the humerus elevates, the peak strain begins on the anterior side as the humeral head is externally rotating (*Figure 5a*), putting the anterior portion under tension. As the humerus elevates, the tendon experiences bending, putting the posterior side under more tension (*Figure 5b*). The maximum effective strain, as calculated in *Equation 3*, in the tendon across the range of motion is shown below (*Figure 6*).

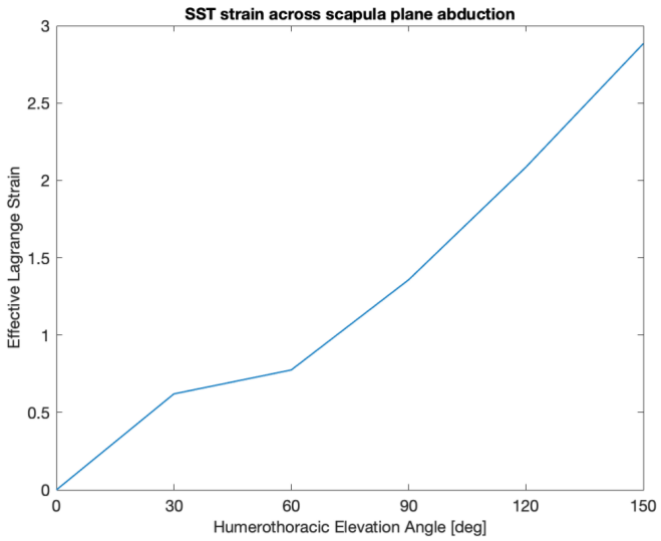

Figure 4. Lagrange Strain of the Supraspinatus Tendon across Arm Elevation

Across the range of motion, it can be seen that the effective strain increases as humerothoracic elevation increases. These strain values are particularly high, which is

likely a result of the use of linear tetrahedral elements, which tend to misrepresent strain, particularly in the case of bending.

Similarly, FEBio calculates the effective stress, as in *Equation 4*, and applies a color map to visualize (*Figure 7*).

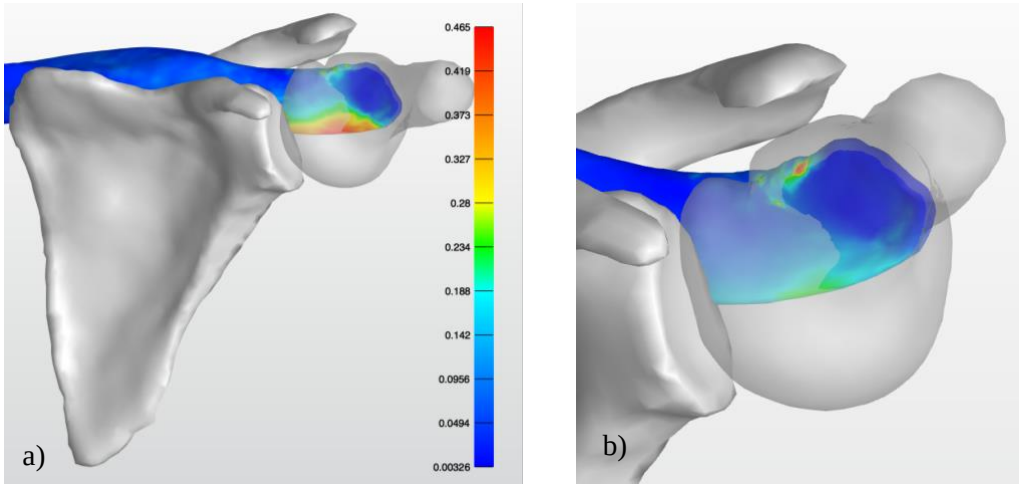

Figure 5. Effective Stress across the Tendon a) at 120˚ of Humerothoracic Elevation (Anterior View). b) at 150˚ of Humerthoracic Elevation.

For most of the range of motion, the maximum stress follows the pattern of the maximum strain. At the beginning of the range of motion, from 30˚ to about 60˚ the anterior portion of the tendon has the peak stress as the humeral head is externally rotating. As the humerus continues to elevate, the posterior portion experiences more tension, resulting in higher stress. At the end range position, the anterior region experiences a stress concentration due to the extreme bending of the tendon. The magnitude of peak stress across the range of arm elevation can be seen in *Figure 8*, below.

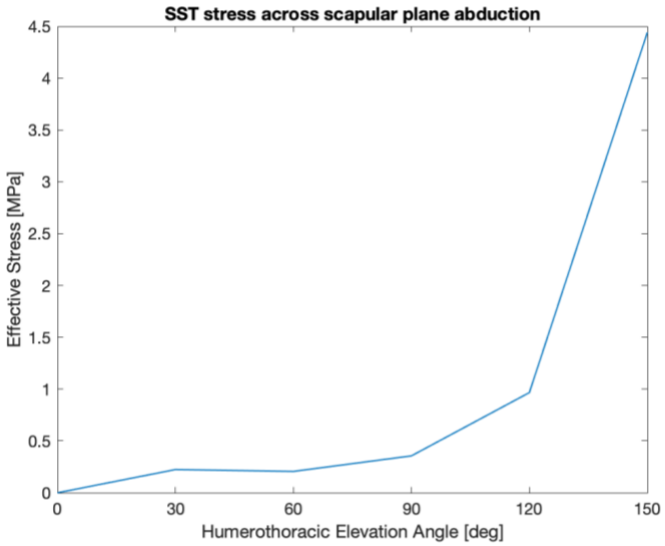

Figure 6. Cauchy Stress of the Supraspinatus Tendon across Arm Elevation

The supraspinatus tendon can be thought of as having a few distinct portions. The footprint of the tendon, where the tendon attaches to the humeral head, and the critical zone, which is one centimeter medial to the footprint of the tendon. These are significant portions of the tendon, as the footprint experiences very high forces as it is the force transmitter from the muscle to the humerus. The critical zone, encompassing the footprint and one centimeter medial, is where tears are most likely to occur [40].

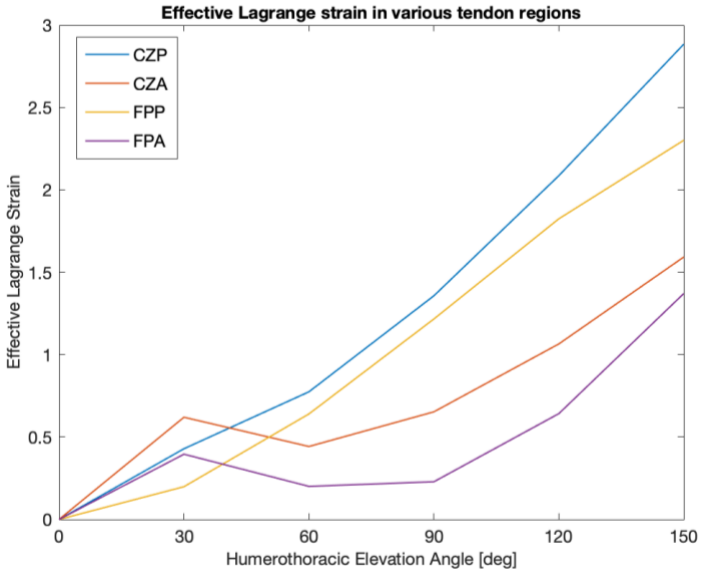

Figure 7. Lagrange Strain in Different Regions of the Tendon across Arm Elevation. CZP and CZA represent the posterior and anterior portions of the critical zone, respectively. Likewise, FPP and FPA

represent the posterior and anterior portions of the footprint of the tendon.

The behavior of the footprint and critical zones are fairly consistent, but the trends are different between anterior and posterior. On the posterior side, the strain increases consistently with elevation angle. On the anterior side, the trend is less direct, with a small peak at 30˚ where the tendon undergoes the initial external rotation.

The effective stress in each portion of the tendon was calculated, and can be seen in *Figure 10*, below.

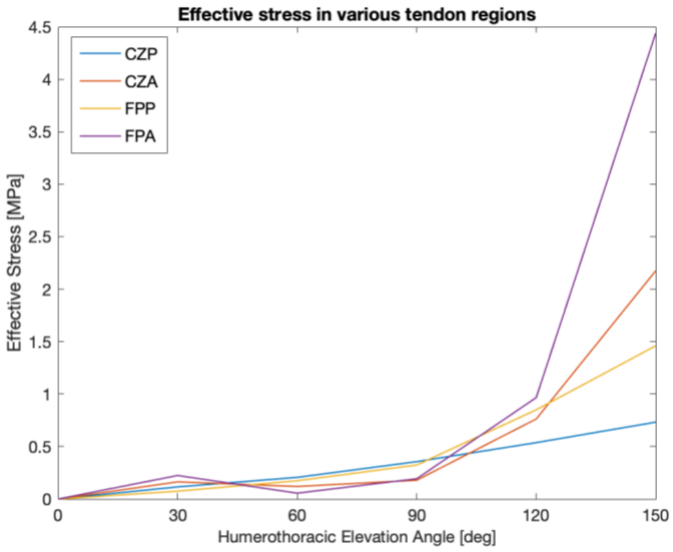

Figure 8. Cauchy Stress in Different Portions of the Tendon across Arm Elevation. CZP and CZA represent the posterior and anterior portions of the critical zone, respectively. Likewise, FPP and FPA represent the posterior and anterior portions of the footprint of the tendon.

Ideally, from an efficiency standpoint, the humeral head would rotate about its axis with no translation of the humeral head. Even in healthy individuals, however, we see translation of the humeral head during motion, ranging between 0 and 5 millimeters in the superior direction [13]. The model was run with translations of two and five millimeters superior and inferior applied linearly throughout the range of motion to compare how these various translations impact supraspinatus mechanics. In the inferior translation cases, the element strain was too large that the model did not run all the way. The effective Lagrange

strain (*Figure 11*), and effective stress (*Figure 12*), for arm elevation from 0˚ to 120˚ can be seen below.

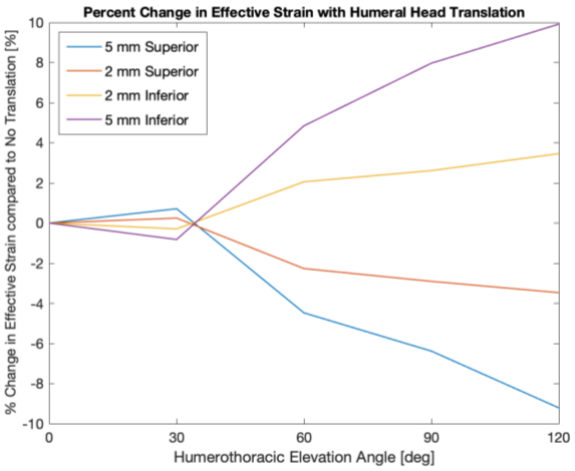

Figure 10. Changes in Lagrange Strain with Varying Humeral Head Translations.

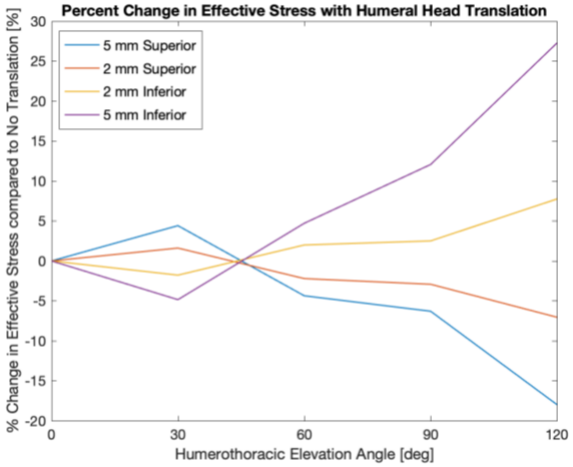

Figure 10. Changes in Effective Stress with Varying Humeral Head T*ranslation.*

As can be seen in the figures above, superior translation tends to decrease maximum stress and maximum strain, while inferior translation tends to increase it.

Discussion

Across arm elevation, both the stress and strain were seen to increase with humerothoracic elevation (*Figures 6* and *8*). Due to the position of the humerus relative to the scapula, the supraspinatus has to twist and bend in order to facilitate that position. This causes fairly high stresses and strains, particularly at end range humerothoracic elevation.

The location of the peak stresses and strains changes across the range of motion as well. At the beginning of motion, from about 0˚ to 30˚, the peak stress and peak strain are on the anterior portion of the tendon. As the humerus externally rotates, the anterior portion of the tendon has to stretch. At further elevations, the tendon bends the other way, causing the posterior portion to contain the peak stresses and strains, which are much higher in magnitude than the anterior portion was exposed to (*Figure 7a*). At the end range of motion, (*Figure 7b*), there is a stress concentration on the anterior portion of the tendon.

This spot, at the footprint of the tendon, likely occurs due to the bending compression of these elements, along with their role in transmitting the force from the muscle to the humerus. This stress concentration may be reduced with increased load, which would keep the tendon experiencing such extreme bending.

Lake et al found that the posterior portion of the supraspinatus tendon had the lowest modulus relative to the anterior and medial portions of the tendon [6]. Although these different material properties were not modeled, the posterior portion of the tendon experiences much higher strains than the anterior portion (*Figure 9*). This may be made possible in reality by its reduced modulus relative to the rest of the tendon, allowing it to deform more without experiencing especially large stresses.

Although there appeared to be a difference in the trend between anterior and posterior tendon mechanics, there was not much difference between the footprint and the critical zone (*Figures 9* and *10*). The critical zone had slightly higher strains than the footprint, while the footprint had higher stresses. The difference between where stresses and strains occur is likely due to the tensile load on the footprint in the axial direction. The fibers limit tensile deformation, but carry a lot of the load, due to their strong nature, while the matrix is able to bend and deform.

When translation is imposed across the range of motion, the mechanics were observed to change in fairly consistent ways. As seen in *Figures 11* and *12*, superior translation causes a decrease in the amount of stress and strain in the tendon, while inferior translation causes an increase. This makes sense, as inferior translation would apply additional traction force on the tendon by the humerus pulling it in the direction opposite the muscle force, adding tension. By the same logic, superior translation reduces this force.

Too much superior translation, though, reduces the subacromial space, and could cause the tendon to come into contact with the coracoacromial arch. There is some optimal amount of superior translation that minimizes the amount of stress in the tendon, without causing subacromial impingement.

Clinical Significance

The results of this model may ultimately be used to assess risk of rotator cuff tear development and inform strategies for prevention. It was found that stress and strain increase at higher arm elevations. Intuitively, increased strain on the tendon may result in microtrauma of the tissue, resulting in increased likelihood for rotator cuff degeneration. People may be in these extreme elevation positions due to occupational requirements, such as those working in labor intensive jobs that require a lot of overhead lifting, such as those in construction fields. They also may reach these positions if they are experiencing limited scapular upward rotation, as they would need to compensate with increased glenohumeral joint elevation. This population may benefit from rehabilitation aimed at increasing scapular upward rotation in order to decrease supraspinatus tendon strain in elevation.

This study found that superior humeral head translation tended to decrease stress and strain on the tendon over the range of motion, while inferior translation increased it. From a clinical standpoint, a patient with shoulder pain may be inferiorly translating their humeral head in an effort to reduce the pain they feel in high elevations, but this motion is actually increasing the strain on the supraspinatus tendon, furthering the problem. These results may indicate that patients with shoulder pain of suspected supraspinatus origin should reduce the amount of time they spend in extreme glenohumeral elevation.

Movement interventions may be prescribed to address issues in scapular kinematics, as well as to optimize humeral head translation across the range of motion.

Assumptions and Limitations

Due to the complexity of biomechanical systems, a number of simplifications must be made in order to create a reasonable finite element model. It is important to consider what the question is, and how these assumptions may impact the results.

This particular model is limited in part by the material definitions. Only one fiber direction was used to model the supraspinatus. In reality, we know that there is a fiber distribution in the supraspinatus tendon [41]. These different fiber directions would reduce the magnitude of stress and strain in the tendon, and may limit some of the bending experienced by the tendon.

Another limitation is that the tendon is modeled as having uniform material properties. In reality, we know that the tendon properties vary from anterior to posterior as well as on the joint or bursal surfaces [6,41]. Similarly, in the model, there is a defined line where the material properties shift from tendon to muscle. In reality there is a gradient of material properties from tendon to muscle. These variable material properties likely do not have a huge effect on how the supraspinatus deforms, but may impact the magnitude of stress in specific regions of the tendon.

The material properties for muscle and tendon were validated previously by modeling a biaxial test from the literature [6]. Using this as a material validation is limited, however, because the validation of two-dimensional behavior does not necessarily translate to the three-dimensional behavior of the tissue.

Another limitation of the model is the definition of the force. The muscle force is

applied to the back of the muscle to simulate force transmission from the muscle to the tendon. A more physiologically accurate representation of this would be to prescribe a uniaxial contraction of the muscle. The applied external force was used because it was most similar to the experimental set up. In reality, the muscle does not apply a constant force across the range of motion, so possibly a more dynamic definition would be appropriate.

The model is further limited by the imposition of average kinematics. Each subject has unique anatomy and kinematics. In this model, average motion was imposed from previous data. A more accurate method would be to measure subject-specific three-dimensional kinematics and apply them to the model.

It is assumed for the purposes of simplicity that the other rotator cuff tendons behave independently of the supraspinatus, and that they hold the humeral head centered throughout the range of motion. When humeral head translation is imposed, it is assumed that translation only occurs in the superior/inferior directions. It is likely that, due to the limited stability of the glenohumeral joint, there is also translation in the anterior/posterior direction.

Future Directions

With the above limitations in mind, the model can certainly be improved. The muscle and tendon were intended to be meshed using quadratic elements using Hypermesh software. These tet10 elements, however, were unable to be implemented in FEBio. In future versions of the model, quadratic tetrahedral elements will be implemented, as they tend to be far more accurate than linear tetrahedral elements, as used in this model.

Future development of the model could include making it more physiologically accurate. More anatomical structures could be modeled, such as the supraspinatus central

tendon [23], the biceps tendon, labrum, other rotator cuff tendons, subacromial bursa, and the coracoacromial ligament. In reality, these structures likely have an impact on each other's mechanical environment. For example, the other rotator cuff tendons are connected by the rotator cuff interval, which causes the tendon forces to be transmitted across the connective tissue. The biceps tendon, labrum, and rotator cuff interval provide passive stability to the joint, which could be utilized to test forces required for subluxation and instability. The coracoacromial ligament provides a ceiling for the tendon, and may be involved with subacromial impingement, which could be modeled with certain subject's anatomy.

More generally, the model can be utilized to answer a number of clinical questions. Various kinematic conditions can be implemented into the model to understand the difference between various motions, for example pure abduction, scapular plane abduction, and pure flexion. Specific joint angles can be implemented to understand the stress and strain across the entire range of shoulder motion [3]. Further, angles from the literature can be utilized to understand the mechanics at play for unique conditions, such as overhead throwing or wheelchair propulsion [42-44]. Patient-specific kinematics may be implemented based on the three-dimensional joint angles that can be measured by fluoroscopy [13,45]. Average kinematics from the literature can be compared to patient specific kinematics to see how the patient may be adapting their kinematics to reduce potential impingement or overall strain. This would be particularly interesting in the case where a subject has pain and may be adapting their motion to alleviate this pain.

Additionally, various subject's anatomy may be incorporated to understand the effect of anatomy on supraspinatus mechanics. Further, statistical shape modeling, which essentially quantifies anatomical variations, can be implemented to understand how

specific variations in anatomy, for example, the different types of acromions (flat, curved, hooked), impact the mechanics acting on the supraspinatus [46]. Specific pathology and surgical interventions may be modeled in order to understand how these interventions impact the load-bearing capacity, and overall tendon health [29,30,47].

The material definitions could be made more complex in future development of the model. More complex definitions of fiber direction and specific muscle pennation could be implemented as in Blemker and Delp, 2005 [36]. Material definitions that incorporate tissue degeneration could be incorporated to investigate intrinsic mechanisms of rotator cuff tears.

The force definition could be improved by doing a forward dynamics experiment to identify the true force of the supraspinatus muscle to produce the motion. This can be done using software like OpenSim (Stanford University). An initial guess is input based on EMG recordings, and the software performs a metabolic optimization to determine how much force each muscle is producing in order to produce a certain motion. The force results from a simulation like this may be useful in prescribing a realistic amount of force on the tendon.

Conclusion

Rotator cuff tears are extremely common, and can be a fairly debilitating injury. The exact causes of rotator cuff pathology are not well understood. This study aimed to see how supraspinatus tendon mechanics vary across a range of arm elevation, and further, to examine how imposing superior and inferior translations of 2 and 5 mm impact the stress and strain. It was found that stress and strain increase across the range of arm elevation, with the posterior portion of the tendon experiencing the greatest amount of strain and the

anterior portion near the footprint of the tendon experiencing the greatest amount of stress. The maximum stress within the tendon decreased with superior humeral head translation, and increased with inferior humeral head translation. Further study is required in order to validate the model. The model has the ability to be extended in order to address numerous clinical questions, and truly understand the complex interaction between morphology and kinematics, and ultimately understand some potential mechanisms of rotator cuff pathology.

Bibliography

1. Neer II CS. Anterior Acromioplasty for the Chronic Impingement Syndrome in the Shoulder: A Preliminary Report. *Annual Meeting of the American Orthopaedic Association.* 1972;54(1):41-50.
2. Browning DG, Desai MM. Rotator cuff injuries and treatment. *Prim Care.* 2004;31(4):807-829.
3. Lawrence RL, Sessions WC, Jensen MC, et al. The effect of glenohumeral plane of elevation on supraspinatus subacromial proximity. *J Biomech.* 2018;79:147-154.
4. Ludewig PM, Phadke V, Braman JP, Hassett DR, Cieminski CJ, LaPrade RF. Motion of the shoulder complex during multiplanar humeral elevation. *J Bone Joint Surg Am.* 2009;91(2):378-389.
5. Bey MJ, Song HK, Wehrli FW, Soslowsky LJ. Intratendinous strain fields of the intact supraspinatus tendon: the effect of glenohumeral joint position and tendon region. *Journal of Orthopaedic Research.* 2012;20:869-874.
6. Lake SP, Miller KS, Elliott DM, Soslowsky LJ. Effect of fiber distribution and realignment on the nonlinear and inhomogeneous mechanical properties of human supraspinatus tendon under longitudinal tensile loading. *J Orthop Res.* 2009;27(12):1596-1602.
7. Ludewig PM, Borstad JD. The Shoulder Complex. In: Company FAD, ed. *Joint Structure and Function.* Vol 5. Philadelphia, PA: Paypee Brothers Medical Publishers; 2011:232,245-257.
8. Picavet HSJ, Schouten JSAG. Musculoskeletal pain in the Netherlands: prevalences, consequences and risk groups, the DMC3-study. *Pain.* 2003;102(1):167-178.
9. Gschwend N, Ivosević-Radovanović D, Patte D. Rotator cuff tear — relationship between clinical and anatomophathological findings. *Arch Orthop Trauma Surg.* 1988;107(1):7-15.
10. Bishop JL, Kline SK, Aalderink KJ, Zauel R, Bey MJ. Glenoid inclination: in vivo measures in rotator cuff tear patients and associations with superior glenohumeral joint translation. *J Shoulder Elbow Surg.* 2009;18(2):231-236.
11. Engelhardt C, Farron A, Becce F, Place N, Pioletti DP, Terrier A. Effects of glenoid inclination and acromion index on humeral head translation and glenoid articular cartilage strain. *J Shoulder Elbow Surg.* 2017;26(1):157-164.
12. Bigliani LU, Morrison DS, April EW. The morphology of the acromion and its relationship to rotator cuff tears. *Orthop Trans.* 1986;10:216.
13. Giphart JE, Brunkhorst JP, Horn NH, Shelburne KB, Torry MR, Millett PJ. Effect of plane of arm elevation on glenohumeral kinematics: a normative biplane fluoroscopy study. *J Bone Joint Surg Am.* 2013;95(3):238-245.
14. Henseler JF, de Witte PB, de Groot JH, van Zwet EW, Nelissen RG, Nagels J. Cranial translation of the humeral head on radiographs in rotator cuff tear patients: the modified active abduction view. *Med Biol Eng Comput.* 2014;52(3):233-240.

15. Büchler P, Farron A. Benefits of an anatomical reconstruction of the humeral head during shoulder arthroplasty: a finite element analysis. *Clinical Biomechanics.* 2004;19(1):16-23.
16. Debski RE, Weiss JA, Newman WJ, Moore SM, McMahon PJ. Stress and strain in the anterior band of the inferior glenohumeral ligament during a simulated clinical examination. *J Shoulder Elbow Surg.* 2005;14(1 Suppl S):24S-31S.
17. Drury NJ, Ellis BJ, Weiss JA, McMahon PJ, Debski RE. Finding consistent strain distributions in the glenohumeral capsule between two subjects: implications for development of physical examinations. *J Biomech.* 2011;44(4):607-613.
18. Drury NJ, Ellis BJ, Weiss JA, McMahon PJ, Debski RE. The impact of glenoid labrum thickness and modulus on labrum and glenohumeral capsule function. *J Biomech Eng.* 2010;132(12):121003.
19. Ellis BJ, Debski RE, Moore SM, McMahon PJ, Weiss JA. Methodology and sensitivity studies for finite element modeling of the inferior glenohumeral ligament complex. *J Biomech.* 2007;40(3):603-612.
20. Ellis BJ, Drury NJ, Moore SM, McMahon PJ, Weiss JA, Debski RE. Finite element modelling of the glenohumeral capsule can help assess the tested region during a clinical exam. *Comput Methods Biomech Biomed Engin.* 2010;13(3):413-418.
21. Favre P, Senteler M, Hipp J, Scherrer S, Gerber C, Snedeker JG. An integrated model of active glenohumeral stability. *J Biomech.* 2012;45(13):2248-2255.
22. Gatti CJ, Maratt JD, Palmer ML, Hughes RE, Carpenter JE. Development and validation of a finite element model of the superior glenoid labrum. *Ann Biomed Eng.* 2010;38(12):3766-3776.
23. Webb JD, Blemker SS, Delp SL. 3D finite element models of shoulder muscles for computing lines of actions and moment arms. *Comput Methods Biomech Biomed Engin.* 2014;17(8):829-837.
24. Barea C, Hobatho MC, Darmana R, Mansat P, Mansat M. Three Dimensional Finite Element Modelling of Normal and Implanted Glenoid: Validations and Simulations. 1998.
25. Farron A, Terrier A, Buchler P. Risks of loosening of a prosthetic glenoid implanted in retroversion. *J Shoulder Elbow Surg.* 2006;15(4):521-526.
26. Duprey S, Bruyere K, Verriest JP. Human shoulder response to side impacts: a finite element study. *Comput Methods Biomech Biomed Engin.* 2007;10(5):361-370.
27. Hadid A, Belzer N, Shabshin N, Zeilig G, Gefen A, Epstein Y. The effect of mechanical strains in soft tissues of the shoulder during load carriage. *J Biomech.* 2015;48(15):4160-4165.
28. Inoue A, Chosa E, Goto K, Tajima N. Nonlinear stress analysis of the supraspinatus tendon using three-dimensional finite element analysis. *Knee Surg Sports Traumatol Arthrosc.* 2013;21(5):1151-1157.
29. Celemín A, Vargas Ariza R, Briceño JC, González Goméz JC, Suárez DR. Influence of Tear Size on the Load Bearing Capacity of the Supraspinatus Tendon. *Ingenieria y Universidad.* 2014;18(2).

30. Engelhardt C, Ingram D, Mullhaupt P, et al. Effect of partial-thickness tear on loading capacities of the supraspinatus tendon: a finite element analysis. *Comput Methods Biomech Biomed Engin.* 2016;19(8):875-882.
31. Sano H, Wakabayashi I, Itoi E. Stress distribution in the supraspinatus tendon with partial-thickness tears: an analysis using two-dimensional finite element model. *J Shoulder Elbow Surg.* 2006;15(1):100-105.
32. Adams CR, Baldwin MA, Laz PJ, Rullkoetter PJ, Langenderfer JE. Effects of rotator cuff tears on muscle moment arms: a computational study. *J Biomech.* 2007;40(15):3373-3380.
33. Grassi L, Vaananen SP, Amin Yavari S, et al. Experimental validation of finite element model for proximal composite femur using optical measurements. *J Mech Behav Biomed Mater.* 2013;21:86-94.
34. Op Den Buijs J, Dragomir-Daescu D. Validated Finite Element Models of the Proximal Femur Using Two-Dimensional Projected Geometry and Bone Density. *Comput Methods Programs Biomed.* 2011;104:168-174.
35. Gardiner JC, Weiss JA. Subject-specific finite element analysis of the human medial collateral ligament during valgus knee loading. *Journal of Orthopaedic Research.* 2003;21:1098-1106.
36. Blemker SS, Delp SL. Three-Dimensional Representation of Complex Muscle Architectures and Geometries. *Annals of Biomedical Engineering.* 2005;33(5):661-673.
37. Massimini DF, Warner JJ, Li G. Glenohumeral joint cartilage contact in the healthy adult during scapular plane elevation depression with external humeral rotation. *J Biomech.* 2014;47(12):3100-3106.
38. Taber LA. Theoretical Mechanobiology. In. St. Louis, MO: Washington University; 2018.
39. Ling S-C, Chen C-F, Wan R-X. A study on the vascular supply of the supraspinatus tendon. *Journal of Clinical Anatomy.* 1990;12(1):161-165.
40. Itoi E, Berglund LJ, Grabowski JJ, et al. Tensile Properties of the Supraspinatus Tendon. *Journal of Orthopaedic Research.* 1995;13:587-584.
41. Lake SP, Miller KS, Elliott DM, Soslowsky LJ. Tensile properties and fiber alignment of human supraspinatus tendon in the transverse direction demonstrate inhomogeneity, nonlinearity, and regional isotropy. *J Biomech.* 2010;43(4):727-732.
42. Plummer H, Oliver GD. Quantitative analysis of kinematics and kinetics of catchers throwing to second base. *J Sports Sci.* 2013;31(10):1108-1116.
43. Wicke J, Keeley DW, Oliver GD. Comparison of pitching kinematics between youth and adult baseball pitchers: a meta-analytic approach. *Sports Biomech.* 2013;12(4):315-323.
44. Bednarczyk JH, Sanderson DJ. Kinematics of Wheelchair Propulsion in Adults and Children With Spinal Cord Injury. *Arch Phys Med Rehabil.* 1994;75(12):1327-1334.
45. Lawrence RL, Ellingson AM, Ludewig PM. Validation of single-plane fluoroscopy and 2D/3D shape-matching for quantifying shoulder complex kinematics. *Med Eng Phys.* 2018;52:69-75.

46. Harris MD, Datar M, Whitaker RT, Jurrus ER, Peters CL, Anderson AE. Statistical shape modeling of cam femoroacetabular impingement. *J Orthop Res.* 2013;31(10):1620-1626.
47. Funakoshi T, Suenaga N, Sano H, Oizumi N, Minami A. In vitro and finite element analysis of a novel rotator cuff fixation technique. *J Shoulder Elbow Surg.* 2008;17(6):986-992.